Available online at www.sciencedirect.com
SCIENCE DIRECT®
International Journal of Heat and Mass Transfer 48 (2005) 4685–4694
International Journal of HEAT and MASS TRANSFER
www.elsevier.com/locate/ijhmt

Numerical study of confined slot jet impinging on porous metallic foam heat sink

Tzer-Ming Jeng [a], Sheng-Chung Tzeng [b,*]

[a] Department of Mechanical Engineering, Air Force Institute of Technology, GangShan 820 Taiwan, ROC
[b] Department of Mechanical Engineering, Chienkuo Technology University, Changhua 500 Taiwan, ROC

Received 25 September 2004; received in revised form 24 June 2005

Abstract

This study numerically investigates the impinging cooling of porous metallic foam heat sink. The analyzed parameters ranges comprise $\varepsilon = 0.93/10$ PPI Aluminum foam, $L/W = 20$, $Pr = 0.7$, $H/W = 2$–8, and $Re = 100$–40,000. The simulation results exhibit that when the Re is low (such as $Re = 100$), the Nu_{max} occurs at the stagnation point (i.e. $X = 0$). However, when the Reynolds number increases, the Nu_{max} would move downwards, i.e. the narrowest part between the recirculation zone and the heating surface. Besides, the extent to which the inlet thermal boundary condition influences the prediction accuracy of the Nusselt number increases with a decreasing H/W and forced convective effect. The application ranges of H/W and Re that the effect of the inlet thermal boundary condition can be neglected are proposed. Lastly, comparing our results with those in other studies reveals that the heat transfer performance of the Aluminum foam heat sink is 2–3 times as large as that without it. The thermal resistance is also 30% less than that of the plate fin heat sink for the same volumetric flow rate and the 5.3 mm jet nozzle width. Therefore, the porous Aluminum foam heat sink enhances the heat transfer performance of impinging cooling.

Keywords: Impinging cooling; Porous metallic foam heat sink; Heat transfer; Thermal resistance

1. Introduction

Recent studies have focused on the heat transfer characteristics of the porous metallic foam heat sinks [1–6], with almost all of them discussing the heat transfer improvement of the porous metallic foam heat sinks under the cross channel flow, or measuring the heat transfer coefficient between the fluid flow and foam structure with experimental methods. However, a more direct cooling mode is to blow air to impinge normally onto the heat sink from a frontal direction. Martin [7], Polat et al. [8], and Jambunathan et al. [9] studied the heat convection between the impinging jet flow and the solid surface. According to their results, the Nusselt number could be increased by narrowing the distance between the jet nozzle and the heating surface, increasing the Reynolds number, or applying the parabolic velocity profile at the exit of jet nozzle. Although the heat transfer between the impinging jet flow and fin heat sinks has received considerable interest [10–15], the

* Corresponding author. Tel.: +886 4 711 1111x3132; fax: +886 4 735 7193.
E-mail addresses: tsc@ctu.edu.tw, tsc33@ms32.hinet.net (S.-C. Tzeng).

0017-9310/$ - see front matter © 2005 Elsevier Ltd. All rights reserved.
doi:10.1016/j.ijheatmasstransfer.2005.06.032

Nomenclature

C_1	parameter for inlet thermal boundary condition, see in Eq. (10)
C_F	inertial coefficient of the porous medium
d	diameter of fiber or sphere of the porous medium (m)
Da	Darcy number (K/W^2)
H	height of the heat sink (m)
h_v	volumetric heat transfer coefficient [W/(m^3 °C)]
K	permeability of the porous medium (m^2)
k	thermal conductivity of fluid [W/(m °C)]
L	length of the heat sink (m)
Nu	Nusselt number at the heating surface (hW/k_f)
Nu_{fs}	fluid-to-solid Nusselt number based on the fiber diameter ($Nu_{fs} = h_v d^2/k_f$)
Nu^*_{fs}	fluid-to-solid Nusselt number based on the jet width ($Nu_{fs} = h_v W^2/k_f$)
Pr	Prandtl number (ν/α)
PPI	pore per inch
Q	flow rate at the jet exit (m^3/min)
R	thermal resistance (°C/W, Eq. (18))
Re	Reynolds number based on the jet velocity and jet width ($\rho_f V_j W/\mu$)
Re_d	Reynolds number based on the local velocity and fiber diameter ($Re_d = \rho_f \sqrt{u^2+v^2} d/\mu$)
T	temperature (°C)
u	velocity in jet transverse direction (m/s)
U	dimensionless velocity in jet transverse direction (u/V_j)
v	velocity in jet streamwise direction (m/s)
V	dimensionless velocity in jet streamwise direction (v/V_j)
W	width of the slot jet nozzle
x, y	Cartesian coordinates
X, Y	dimensionless Cartesian coordinates (x/W, y/W)
Δp	pressure drop (Pa)

Greek symbols

ε	porosity or void fraction of the porous medium
μ	viscosity
θ	dimensionless temperature [$(T - T_j)/(T_w - T_j)$]
ρ	density
ω	vorticity
Ψ	stream function

Subscripts

d	thermal dispersion
D	hydraulic diameter of the jet nozzle
f	fluid
j	jet nozzle
max	maximum
s	solid or stagnation
w	channel wall

Superscript

*	equivalent

impinging cooling of the porous metallic foam heat sinks has seldom been studied.

Fu and Huang [16] numerically investigated the thermal performances of various shape porous blocks under the fully unconfined slot jet. They employed the empirical formula of porous properties of a packed spherical bed in solving momentum equation. Additionally, they assumed that the fluid and porous medium is at local thermal equilibrium, then the one-equation model could be utilized to build an energy equation. Their study results indicated that the key element that affect the total performance of porous blocks is the amount of flow that gets close to the heating surface. Restated, more blowing fluid that accesses the porous medium and reaches the heating surface implies a more improved performance. Relevant effect factors include the ratio of the tip gap to the the jet nozzle width, the shape of the porous medium, the porous medium type and the fluid type, the velocity profile at the outlet of jet nozzle, and the Reynolds number. Fu and Huang [16] only mentioned the Reynolds number to derive the shape of the porous medium with the optimum thermal performance. Other than, building an energy equation with the one-equation model when the fluid and the porous medium has not yet reached local thermal equilibrium would misjudge the heat transfer performance and the influence of the inlet thermal boundary condition on the numerical simulation would be ignored. Conversely, the influence of the inlet thermal boundary condition should not be neglected, particularly when the Reynolds number is low. Hwang et al. [17], Jeng and Hung [18] have already proposed this notion.

This work discusses how the height of the aluminum foam heat sink and the Reynolds number influence the flowing characteristic and the Nusselt number to demonstrate a primary understanding. Especially the two-

equation model is applied in the numerical simulation, which would bring a more exact predication on the heat transfer performance when the Reynolds number is low. A systematical investigation is also performed to understand how the inlet thermal boundary condition influences the numerical simulation. Finally, a comparison with the plate fin heat sink is made to more thoroughly understand the heat transfer enhancement of the porous metallic foam heat sink during impinging cooling.

2. Numerical model

2.1. Basic assumptions and governing equations

Fig. 1 illustrates a physical configuration of this study. The aluminum foam heat sinks are positioned on the sealed module of multi-chips and restricted within a rectangular channel made of the thermal insulating material. A slot jet is located above the channel from which the air is blown for impinging cooling. While the two sidewalls of the channel are thermal insulating, the entire structure can be simplified as a two-dimensional issue. Fig. 2 depicts the computational configuration of this study and assumes the symmetrical computing domain. L and W, respectively denote the length of the heat sink and the width of the slot jet. H signifies the height of the heat sink and there is no gap between the heat sink and the top wall of the channel. The blown air has a uniform velocity and temperature, and the heating surface is isothermal. To assist the numerical simulation of this issue, the following assumptions are also made: (1) the structure of the porous medium is homogenous and isotropic; (2) the fluid flow is in a steady state, laminar and incompressible; (3) the thermophysical properties of the fluid and porous media are invariant; (4) the local non-thermal equilibrium between

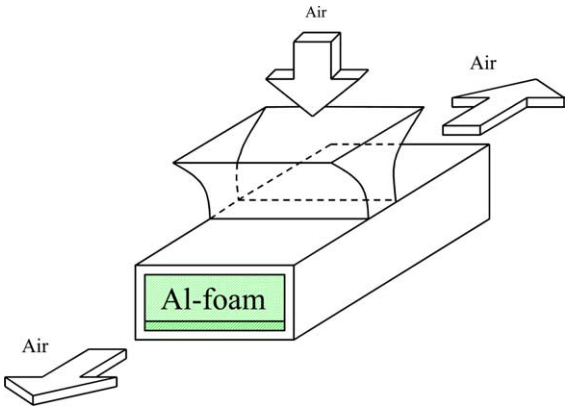

Fig. 1. Physical configuration.

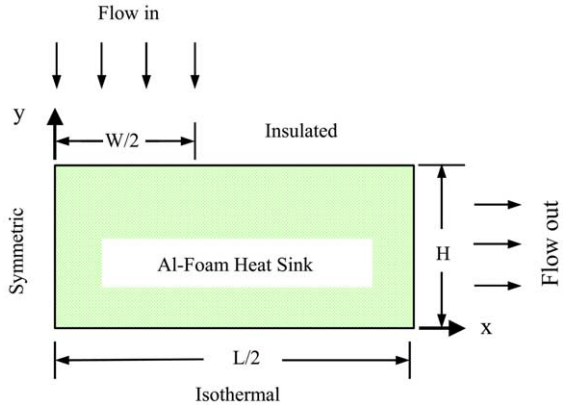

Fig. 2. Computational configuration.

the porous medium and fluid stream exists. Besides, the dimensionless parameters are adopted as following:

$$X=\frac{x}{W},\quad Y=\frac{y}{W},\quad U=\frac{u}{V_j},\quad V=\frac{v}{V_j},\quad Pr=\frac{v_f}{\alpha_f},$$
$$P=\frac{p}{\rho_f V_j^2},\quad Da=\frac{K}{W^2},\quad Re=\frac{\rho_f V_j W}{\mu},$$
$$U_M=\frac{\sqrt{u^2+v^2}}{V_j},\quad \theta=\frac{T-T_j}{T_w-T_j},\quad Nu_{fs}^*=\frac{h_v W^2}{k_f} \tag{1}$$

meanwhile the vorticity (ω) and the stream function (Ψ) are introduced as

$$\omega=-\frac{\partial U}{\partial Y}+\frac{\partial V}{\partial X},\quad U=\frac{\partial \Psi}{\partial Y},\quad V=-\frac{\partial \Psi}{\partial X} \tag{2}$$

then, the following dimensionless equations are obtained:

$$-\omega=\frac{\partial^2\Psi}{\partial X^2}+\frac{\partial^2\Psi}{\partial Y^2} \tag{3}$$

$$U\frac{\partial\omega}{\partial X}+V\frac{\partial\omega}{\partial Y}=-\frac{\varepsilon^2}{ReDa}\omega-\frac{\varepsilon^2 C_F U_M}{\sqrt{Da}}\omega+\frac{\varepsilon^2 C_F}{\sqrt{Da}}\left(U\frac{\partial U_M}{\partial Y}-V\frac{\partial U_M}{\partial X}\right)+\frac{\varepsilon}{Re}\left(\frac{\partial^2\omega}{\partial X^2}+\frac{\partial^2\omega}{\partial Y^2}\right) \tag{4}$$

$$U\frac{\partial\theta_f}{\partial X}+V\frac{\partial\theta_f}{\partial Y}=\frac{Nu_{fs}^*}{RePr}(\theta_s-\theta_f)+\frac{1}{RePr}\left\{\frac{\partial}{\partial X}\left[\left(\frac{k_f^*+k_d}{k_f}\right)\frac{\partial\theta_f}{\partial X}\right]+\frac{\partial}{\partial Y}\left[\left(\frac{k_f^*+k_d}{k_f}\right)\frac{\partial\theta_f}{\partial Y}\right]\right\} \tag{5}$$

$$0=Nu_{fs}^*(\theta_f-\theta_s)+\frac{k_s^*}{k_f}\left(\frac{\partial^2\theta_s}{\partial X^2}+\frac{\partial^2\theta_s}{\partial Y^2}\right) \tag{6}$$

2.2. Boundary conditions

Relevant boundary conditions are shown as follows:

$$\Psi = 0, \quad \omega = 0, \quad \frac{\partial \theta_f}{\partial X} = \frac{\partial \theta_s}{\partial X} = 0 \quad \text{for } X = 0 \tag{7}$$

$$\frac{\partial^2 \Psi}{\partial X^2} = 0, \quad \frac{\partial \omega}{\partial X} = 0, \quad \frac{\partial \theta_f}{\partial X} = 0,$$

$$Nu^*_{fs}(\theta_s - \theta_f) = \frac{k^*_s}{k_f}\left(\frac{\partial^2 \theta_s}{\partial Y^2}\right) \quad \text{for } X = L/(2W) \tag{8}$$

$$\Psi = 0, \quad \omega = \frac{-\partial^2 \Psi}{\partial Y^2}, \quad \theta_f = \theta_s = 1 \quad \text{for } Y = 0 \tag{9}$$

$$\Psi = X, \quad \omega = \frac{-\partial^2 \Psi}{\partial Y^2}, \quad \theta_f = 0,$$

$$\frac{k^*_s}{k^*_f + k_d}\frac{\partial \theta_s}{\partial Y} = C_1 \frac{W}{d}\left(Re\frac{d}{W}\right)^{0.5}(\theta_f - \theta_s)$$

$$\text{for } Y = H/W \text{ and in-flow surface} \tag{10}$$

$$\Psi = 0.5, \quad \omega = \frac{-\partial^2 \Psi}{\partial Y^2}, \quad \frac{\partial \theta_f}{\partial Y} = \frac{\partial \theta_s}{\partial Y} = 0$$

$$\text{for } Y = H/W \text{ and insulated surface} \tag{11}$$

At the in-flow surface, the heat convection between the fluid and solid is assumed to be the impinging jet flow. A similar form of the local heat transfer rate at the in-flow surface like as that reported by Ma and Bergles [19] is then applied in Eq. (10). The C_1 (see Eq. (10)) is a parameter for the inlet thermal boundary condition and will be discussed in the Results and discussion section.

2.3. Thermophysical properties

Table 1 presented the porous properties of aluminum foam heat sinks studied herein, including the permeability (K) used in Eqs. (1) and (4), the inertial coefficient (C_F) used in Eq. (4), the empirical correlation of fluid-to-solid Nusselt number ($Nu_{fs} = h_v d^2/k_f$) used in Eqs. (1), (5), (6) and (8) and others. The K and C_F values were determined by the method described by Hunt and Tien [1]. The volumetric heat transfer coefficient between the aluminum foam and the cooling fluid (h_v) was measured by Jeng et al. [6] employing the single-blow method. Moreover, the values of k^*_f and k^*_s employ the empirical formula proposed by Calmidi and Mahajan [20].

Table 1
Relative properties of porous aluminum foam heat sinks (Jeng et al. [6])

Specimens	(a)	(b)	(c)
ε	0.93	0.93	0.93
PPI	10	20	40
d [mm]	0.4	0.21	0.11
K [m^2]$\times 10^{-8}$	7.838	5.308	2.717
C_F	0.019	0.020	0.020
$C = Nu_{fs}/Re_d^{1.277}$	1.77×10^{-3}	2.49×10^{-3}	6.22×10^{-3}

Note: $Re_d = \rho_f\sqrt{u^2+v^2}d/\mu$, $Nu_{fs} = h_v d^2/k_f$.

$$k^*_f = \varepsilon k_f \tag{12}$$

$$k^*_s = 0.181(1-\varepsilon)^{0.763}k_s \tag{13}$$

Relevant thermal dispersion conductivity adopts the empirical formula revised by Calmidi and Mahajan [4].

$$k_d = 0.06RePr\sqrt{Da}U_M k_f \tag{14}$$

3. Numerical procedure and data reduction

This study employs the power-law to disperse the equations and uses the SIS solver proposed by Lee [21] to resolve related dispersed equations. The numerical procedure initially resolves the vorticity and the stream function by alternant iterations, then uses the vorticity and the stream function to resolve the velocity field, which is subsequently substituted into the fluid energy equation. Additionally, the solid and fluid energy equations are solved by alternant iterations and then the solid and fluid temperature fields are acquired. All of the resolutions are subject to the grid test and convergent test. Owing to the large variation in the H/W value, the grid system is divided into four types to fit the physical model. The grid points, in an $x-y$ coordinate system, are 125×51, 125×101, 125×151, and 125×201, respectively. The grid size decreases with a smaller H/W value. The grid size test was conducted, thus confirming the accuracy and consistency of the calculation results for various grid systems. Table 2 lists the results of the grid-dependence test. The relative differences of Ψ values at the specific point are with $\pm0.03\%$ at $Pr = 0.7$ and $Re = 4000$. The iteration is terminated when the variables satisfy the criterion as

$$\sum_{i,j}\left|\frac{F^{n+1}_{i,j} - F^n_{i,j}}{F^{n+1}_{i,j}}\right| \leqslant 5\times10^{-5} \tag{15}$$

where F represents Ψ, ω, and θ. The subscripts i and j show the ith and the jth grid in x and y direction, respectively. The superscript n indicates the nth iteration.

Major parameters of heat transfer performance observed in this study are the Nusselt number and thermal resistance, which are respectively defined as follows:

$$Nu = \frac{hW}{k_f} = -\frac{k^*_f}{k_f}\left(\frac{\partial \theta_f}{\partial Y}\right)_{Y=0} - \frac{k^*_s}{k_f}\left(\frac{\partial \theta_s}{\partial Y}\right)_{Y=0} \tag{16}$$

$$\overline{Nu} = \frac{2W}{L}\int_0^{L/2W} Nu\,dX \tag{17}$$

$$R = \frac{1}{\overline{Nu}}\frac{W}{k_f L^2} \tag{18}$$

Table 2
Grid-dependence test at $Pr = 0.7$ and $Re = 4000$

	$H/W = 2$		$H/W = 4$		$H/W = 6$		$H/W = 8$	
Grid size	61×25	125×51	61×33	125×101	61×51	125×151	61×71	125×201
Ψ	0.4504	0.4505	0.4503	0.4505	0.4503	0.4506	0.4505	0.4508

4. Results and discussion

This study takes a porous aluminum foam heat sink with $\varepsilon = 0.93$ and a pore density of 10PPI (pore per inch). Aluminum foams (Fig. 3) are typically available in high porosities ($\varepsilon > 0.9$) and have an open-celled structure. The ratio of the heat sink length to the jet nozzle width (L/W) equals 20. The jet nozzle width (W) is 5 mm and the Prandtl number (Pr) is 0.7. The parameters of interest in the study are the ratio of the heat sink height to the jet nozzle width (H/W) and the Reynolds number (Re). The ranges of these two parameters are $H/W = 2$–8 and $Re = 100$–40,000. Notably, the jet Reynolds number used in the present study is up to 40,000. In the pure fluid region, the condition of the flow pattern should be turbulent. However, as noted by Antohe and lage [22], the nature of turbulence in porous media is still a controversial issue. Besides, according to the impinging round jet studies in a cylindrical enclosure with a porous foam layer reported by Prakash et al. [23], there are few changes for the flow patterns ($Re = 19{,}000$ and 30,000) in the porous region predicted by two different turbulence models and a laminar model. Since the present system does not have any pure fluid region, using a laminar model to simulate the fluid flow and thermal behavior in the porous region with a large Re is still valuable.

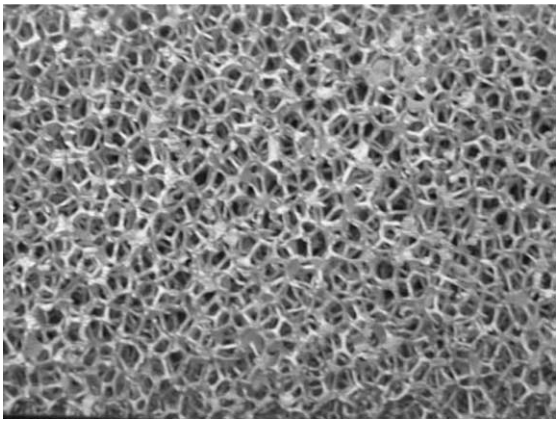

Fig. 3. Picture of a typical aluminum foam sample ($\varepsilon = 0.93$/10PPI).

4.1. Effect of H/W and Re on flowing characteristic

Fig. 4 depicts the contour map of the stream function with $H/W = 2$ and various Reynolds numbers, indicating that a low Reynolds number causes the impinging jet flow to flow smoothly along the jet transverse direction. When the Reynolds number increases, more fluid can penetrate the porous structure of aluminum foam to reach near the heating surface, subsequently forming a recirculation zone. Notably, the effective flowing channel is located between the recirculation zone and the heating surface. Additionally, the narrowest part of the effective flowing channel would have the best heat transfer effect due to the acceleration effect of cooling fluid. This phenomenon is more noteworthy as the Reynolds number increases. The fluid that flows along the jet transverse direction would expand gradually and become uniform within the entire bounded channel. From the characteristic of this fluid flow it indicates: when H/W and Re are fixed, a larger recirculation zone implies

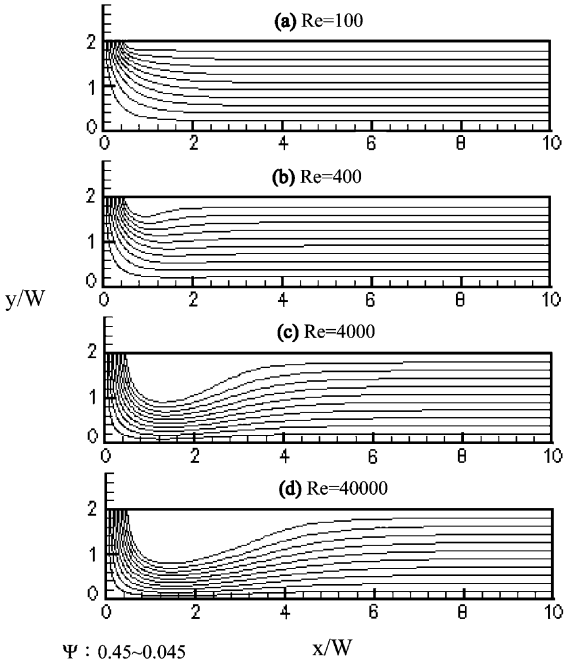

Fig. 4. Stream function contours at $H/W = 2$ for various Reynolds number.

an enhanced heat transfer effect. However, a larger recirculation zone also implies a larger permeability (K) or a larger porosity, the limiting case is without heat sink; and a larger permeability decreases the extended thermal dispersion surface. Therefore, the heat sinks, as H/W and Re are fixed, should exist a most favorable porosity and pore density for maximum cooling performance. Fig. 5 shows the stream function chart at $H/W = 2$ and $H/W = 8$ for $Re = 4000$, indicating that decreasing the H/W increases the turning acceleration and the velocity in the jet transverse direction. However, bigger H/W would also yield a larger extended thermal dispersion surface. Therefore, for the fixed porosity, pore density and Re, the heat sink should also exist an optimal H/W value for the best heat transfer performance. Fig. 6 is provided to investigate the dimensionless temperature distribution. The typical system at $H/W = 2$ and 8 for the maximum Reynolds number ($Re =$ 40,000) is employed. From the contour maps, it demonstrates that the fluid temperature distribution is different from the solid temperature distribution. So the system is not under a local thermal equilibrium condition for the ranges of parameters studied herein. Therefore, the simulations by using a two-equation model may not suit for the present system.

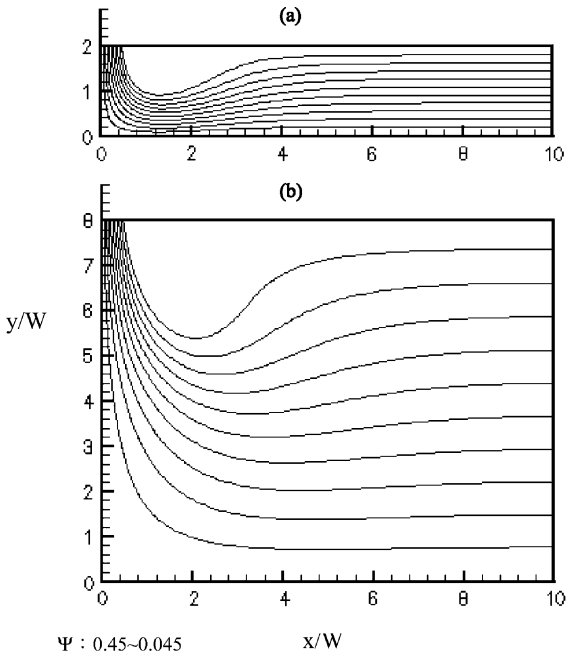

Fig. 5. Stream function contours at $H/W = 2$ and $H/W = 8$ for $Re = 4000$.

4.2. Effect of inlet thermal boundary condition on predicting Nu

Fig. 7 shows the variation in distributions of the Nusselt number along the jet transverse direction for different H/W and Re. A low Reynolds number (e.g., $Re = 100$) causes the maximum Nusselt number to reach the stagnation point (i.e. $X = 0$). An increasing Reynolds number causes the maximum Nusselt number to move downwards. This point is also the narrowest part between the recirculation zone and the heating surface. This can be confirmed in Figs. 4 and 5. The influence of the inlet thermal boundary condition on the numerical prediction would then be examined. C_1 (see Eq. (10)) is the parameter for the inlet thermal boundary condition. A situation in which $C_1 = 0$ implies that the solid–fluid interface at the inlet is in adiabatic condition.

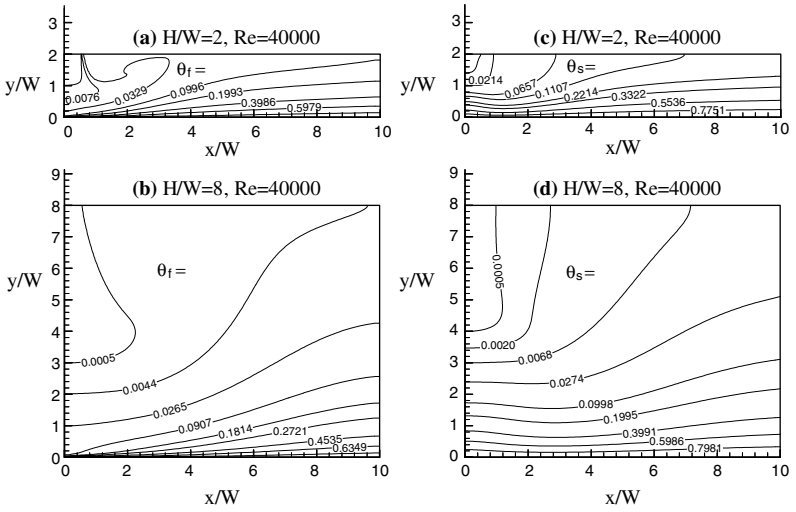

Fig. 6. Dimensionless temperature contours at $H/W = 2$ and $H/W = 8$ for $Re = 40{,}000$ (θ_f as (a) and (b), θ_s as (c) and (d)).

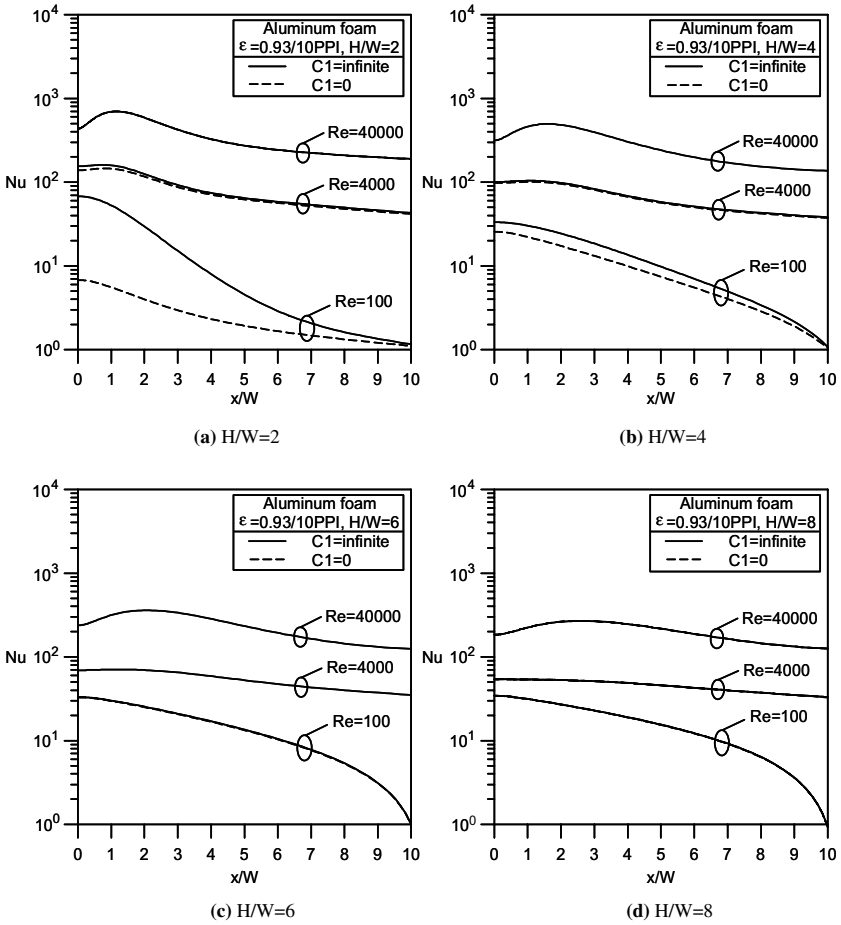

Fig. 7. Heat transfer distribution along jet transverse direction for various Reynolds number and H/W.

Additionally, C_1 tends to be infinite, implying that the solid and the fluid have reached local thermal equilibrium. These are two limiting conditions. Fig. 7 reveals that when H/W and Re decrease, the numerical predictions of the Nusselt number deviate further under these two limiting conditions. Although the assumption that C_1 tends to be infinite is common, Hwang et al. [17], Jeng and Hung [18] proved the conditions that the solid conduction heat transfer is equal to the convective heat transfer between solid and fluid at the inlet is reasonable (which is between the two limiting conditions). This study sets $E(\%)$ as the deviation percentage due to the inlet thermal boundary condition and defines it as

$$E(\%) = \frac{(Nu_s)_{c1=\infty} - (Nu_s)_{c1=0}}{(Nu_s)_{c1=\infty}} \times 100\% \qquad (19)$$

where $(Nu_s)_{c1} = \infty$ means the stagnation Nusselt number for the assumption of $\theta_f = \theta_s$ at the flow-in surface and $(Nu_s)_{c1} = 0$ presents the stagnation Nusselt number for the assumption of $\partial\theta_s/\partial Y = 0$ at the flow-in surface.

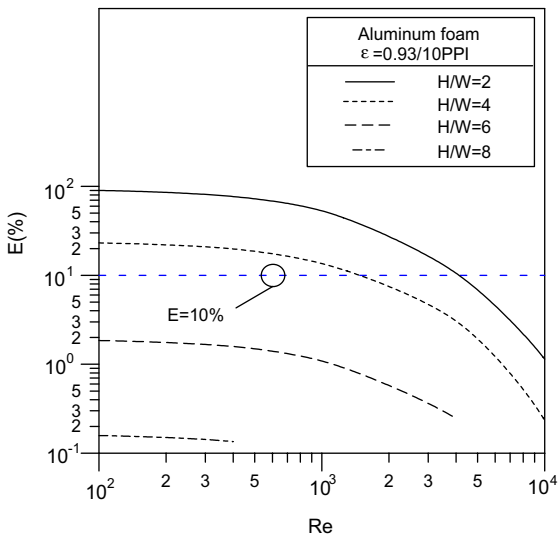

Fig. 8. $E(\%)$ variations with Reynolds number for various H/W.

Fig. 8 illustrates the change of $E(\%)$ dependent on Re at various H/W. Take $E(\%) < 10\%$ which is acceptable, the range that the inlet thermal boundary condition not influencing the numerical prediction is: if $H/W = 2$, $Re > 4000$; if $H/W = 4$, $Re > 1500$; and if $H/W = 6$ and $H/W = 8$, then no influence on Re exists.

4.3. Effect of H/W and Re on Nu_s, Nu_{max} and $\overline{Nu}$

According to above discussion, the range that the inlet thermal boundary condition not influencing the prediction of the Nusselt number is $Re > 4000$ for $H/W =$ 2–8. Therefore, if the inlet thermal boundary condition is uncertain, the discussion extent is limited to $Re > 4000$. To observe how H/W and Re influence the stagnation point Nusselt number (Nu_s) and the maximum Nusselt number (Nu_{max}), this study induces the correlations of Nu_s and Nu_{max} as

$$Nu_s = 4.02(H/W)^{-0.7}Re^{0.5} \tag{20}$$

$$Nu_{max} = 0.75(H/W)^{-0.7}Re^{0.7} \tag{21}$$

The average error deviations of Eqs. (20) and (21) are 11.1% and 9.3%, respectively. The stagnation point Nusselt number (Nu_s) and the maximum Nusselt number (Nu_{max}) increase with a rising Re or decreasing H/W. Furthermore, Gardon and Akfirat [24] examined the impinging cooling of the unconfined slot jet flow without a heat sink and yielded the correlation for the stagnation point Nusselt number (Nu_s) as

$$Nu_s = 1.73(H/W)^{-0.62}Re^{0.58} \tag{22}$$

The scope of application is $H/W = 15$–50 and Re=1905–20,955. Plotting (20) through (22) shown in Fig. 9 reveals that Nu_s and $Nu_{max}$with the porous aluminum foam heat sink are 2–3 times as large as that without the heat sink. Therefore, the impinging cooling performance could be effectively improved with the porous aluminum foam heat sink. The average Nusselt number value ($\overline{Nu}$) is enhanced and benchmarked by the fluid FC-72 slot jet impinging cooling by Wadsworth and Mudawar [25] and the following empirical correlation is made

$$\overline{Nu}_L/Pr^{1/3} = 3.06Re_D^{0.5} + 0.099Re_D^{0.664}[(L-W)/W]^{0.664} \tag{23}$$

The scope of application is $H/W = 1$–20, $(L-W)/W = 24$–99 and $Re_D = 1000$–$30{,}000$. The present numerical study also stimulates a correlation of $\overline{Nu}$ as follows:

$$\overline{Nu} = 0.862(H/W)^{-0.442}Re^{0.6} \tag{24}$$

The average error deviation of Eq. (24) is 10.2%. Eqs. (23) and (24) are included in Fig. 10 and $\overline{Nu}$ with the aluminum foam heat sink are 2–4 times as large as that without it.

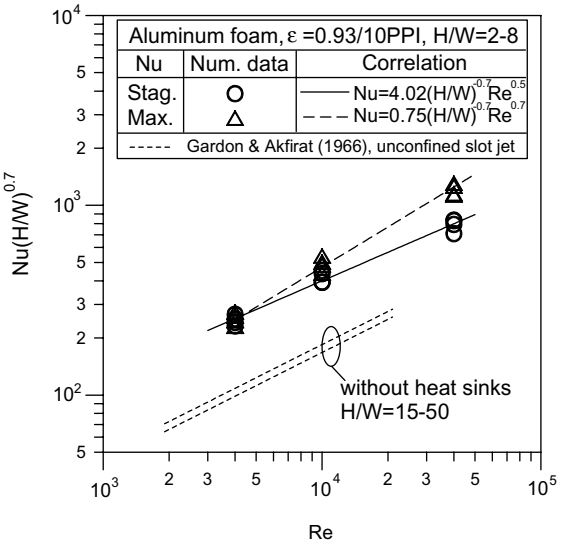

Fig. 9. Stagnation point and maximum Nu variations with Reynolds number for various H/W.

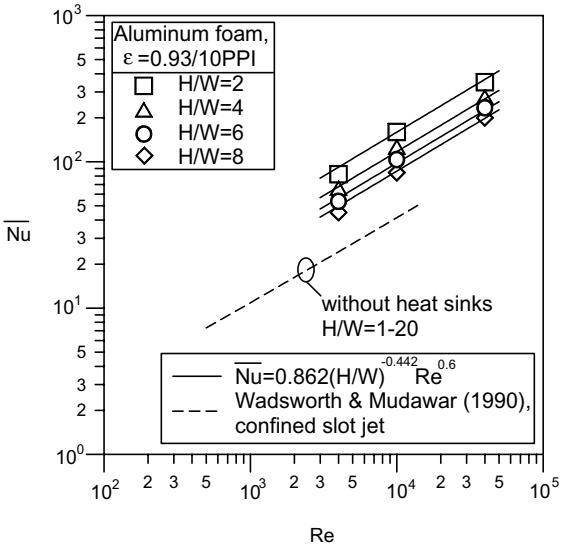

Fig. 10. $\overline{Nu}$ variations with Reynolds number for various H/W.

4.4. Comparison with the thermal performance of the plate fin heat sink

Kondo et al. [12] evaluated the thermal performance of the plate fin heat sink under a confined slot jet. The plate fin heat sink they employed in the test had a width and length of 60 mm, the height and thickness of the fin are 8 and 1 mm, respectively. The interval between fins is 2.7 mm (about 0.72 porosity). The widths of the jet nozzle are 1.3 mm and 5.3 mm. Since that study also exam-

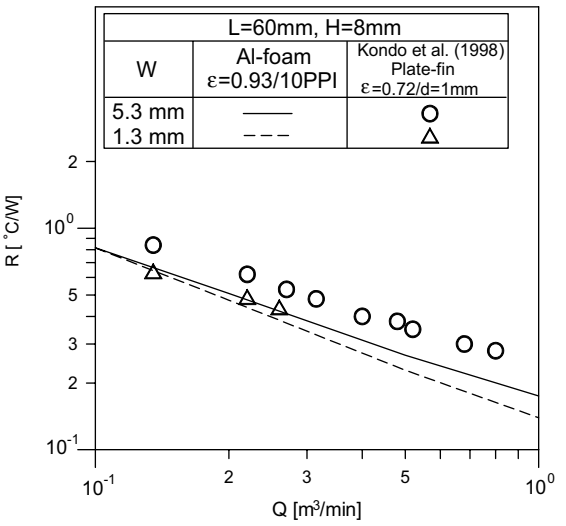

Fig. 11. Comparisons of thermal performance on aluminum foam and plate-fin heat sink.

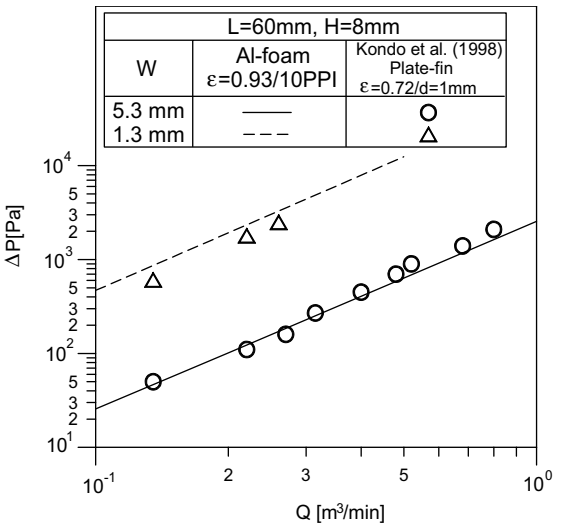

Fig. 12. Comparisons of pressure drop on aluminum foam and plate-fin heat sink.

ines the impinging cooling of the slot jet, therefore its experimental results are ideal for benchmarking. The comparative results of thermal performance are shown in Fig. 11. The heat transfer performance of the porous aluminum foam heat sink is more improved than that of the plate fin heat sink. For example, as the width of the jet nozzle is 5.3 mm, the thermal resistance of the porous aluminum foam heat sink is 30% less than that of the plate fin heat sink. Besides, the rise of pressure drop is an important factor when using a porous material for heat transfer enhancement. The total pressure drop is contributed by the jet nozzle and the porous material. The pressure drop from the jet nozzle can be estimated by using the correlation in the zonal model reported by Kondo et al. [12]. The pressure drop from the porous material can be predicted by integrating the pressure gradient along the symmetric line and the bottom channel wall. Therefore, the total pressure drop is

$$\Delta p = 0.75\rho_f V_j^2 + \rho_f V_j^2 \left[- \int_0^{L/2\ W} \frac{1}{\varepsilon Re} \left\langle \frac{\partial \omega}{\partial Y} \right\rangle_{Y=0} \mathrm{d}x \right] \tag{25}$$

Fig. 12 depicts that the comparative results of pressure drop. The data presents that the pressure drop of the porous aluminum foam heat sink is 10% more than that of the plate fin heat sink for the same volumetric flow rate and the 1.3 mm jet nozzle width. However, the pressure drop of the porous aluminum foam heat sink is quit consistent with that of the plate fin heat sink for the same volumetric flow rate and the 5.3 mm jet nozzle width, indicating that the pressure drop is primarily from the jet nozzle as the flow rate is Q (m^3/min) = 0.1–1.0.

5. Conclusions

This study numerically simulates the impinging cooling of the porous aluminum foam heat sink in the two-equation model. The simulation material is a porous aluminum foam heat sink with $\varepsilon = 0.93$ and a pore density of 10PPI. The ratio of the heat sink length to the jet nozzle width (L/W) equals 20 and the Prandtl number (Pr) is 0.7. The discussed parameters include $H/W = 2$–8 and $Re = 100$–40,000. Based on the results of this study, we conclude the following:

1. A low Reynolds number (e.g., $Re = 100$) causes the maximum Nusselt number to reach the stagnation point (i.e. $X = 0$). However, when the Reynolds number increases, the maximum Nusselt number moves downwards, i.e. the narrowest part between the recirculation zone and the heating surface.
2. When H/W and Re decrease, the inlet thermal boundary condition significantly influences the numerical prediction accuracy of the Nusselt number. Take $E(\%) < 10\%$ which is acceptable, the scope in which the inlet thermal boundary condition does not influence the prediction accuracy of the Nusselt number is: if $H/W = 2$, $Re > 4000$; if $H/W = 4$, $Re > 1500$; if $H/W = 6$ and $H/W = 8$, then there is no influence on Re.
3. The Nusselt number with the porous aluminum foam heat sink is 2–3 times as large as that without it. The thermal resistance of the porous aluminum foam heat sink is 30% less than that of the plate fin heat sink for the same volumetric flow rate and the 5.3 mm jet nozzle width. Therefore, the porous aluminum foam

heat sink can enhance the heat transfer performance of impinging cooling.

References

[1] M.L. Hunt, C.L. Tien, Effects of thermal dispersion on forced convection in fibrous media, Int. J. Heat Mass Transfer 31 (1988) 301–309.

[2] L.B. Younis, R. Viskanta, Experimental determination of the volumetric heat transfer coefficient between stream of air and ceramic foam, Int. J. Heat Mass Transfer 36 (1993) 1425–1434.

[3] K. Ichimiya, A new method for evaluation of heat transfer between solid material and fluid in a porous medium, ASME J. Heat Transfer 121 (1999) 978–983.

[4] V.V. Calmidi, R.L. Mahajan, Forced convection in high porosity metal foams, ASME J. Heat Transfer 122 (2000) 557–565.

[5] J.J. Hwang, G.J. Hwang, R.H. Yeh, C.H. Chao, Measurement of interstitial convection heat transfer and frictional drag for flow across metal foams, ASME J. Heat Transfer 124 (2002) 120–129.

[6] T.M. Jeng, M.P. Wang, G.J. Hwang, Y.H. Hung, Flow resistance and fluid-solid heat exchange in porous metallic foam heat sinks, in: Proceedings of International Symposium on Experimental Mechanics, Taipei, Taiwan, ROC, December 28–30, 2002.

[7] H. Martin, Heat and mass transfer between impinging gas jets and solid surfaces, Advances in Heat Transfer, 13, Academic Press, New York, 1977, pp. 1–60.

[8] S. Polat, B. Huang, A.S. Mujumdar, W.J.M. Douglas, Numerical flow and heat transfer under imping jets: a review, in: C.L. Tien, T.C. Chawia (Eds.), Annual Review of Numerical Fluid Mechanics and Heat Transfer, 2, Hemisphere Publishing Corp., 1989, pp. 157–197.

[9] K. Jambunathan, E. Lai, M.A. Moss, B.L. Button, A review of heat transfer data for single circular jet impingement, Int. J. Heat Fluid Flow 13 (1992) 106–115.

[10] L. Ledezma, A.M. Morega, A. Bejan, Optimal spacing between pin fins with impinging flow, ASME J. Heat Transfer 118 (1996) 570–577.

[11] S. Sathe, K.M. Kelkar, K.C. Karki, C. Tai, C. Lamb, S.V. Patankar, Numerical prediction of flow and heat transfer in an impingement heat Sink, ASME J. Electron. Packaging 119 (1997) 58–63.

[12] Y. Kondo, M. Behnia, W. Nakayama, H. Matsushima, Optimization of finned heat sinks for impingement cooling of electronic packages, ASME J. Electron. Packaging 120 (1998) 259–266.

[13] L.A. Brignoni, S.V. Garimella, Experimental optimization of confined air jet impingement on a pin fin heat sink, IEEE Trans. Components Packaging Technol. 22 (1999) 399–404.

[14] Y. Kondo, H. Matsushima, T. Komatsu, Optimization of pin–fin heat sinks for impingement cooling of electronic packages, ASME J. Electron. Packaging 122 (2000) 240–246.

[15] J.G. Maveety, H.H. Jung, Heat transfer from square pin–fin heat sinks using air impingement cooling, IEEE Trans. Components Packaging Technol. 25 (2002) 459–469.

[16] W.S. Fu, H.C. Huang, Thermal performances of different shape porous blocks under an impinging jet, Int. J. Heat Mass Transfer 40 (1997) 2261–2272.

[17] G.J. Hwang, C.C. Wu, C.H. Chao, Investigation of non-Darcian forced convection in an asymmetrically heated sintered porous channel, ASME J. Heat Transfer 117 (1995) 725–732.

[18] T.M. Jeng, Y.H. Hung, Algorithm for predicting local heat transfer in porous channels by using fin theory, in: Proceedings of the 20th National Conference on Mechanical Engineering, CSME, Taipei, Taiwan, December 5–6, 2003, pp. 1119–1126.

[19] C.F. Ma, A.E. Bergles, Convection heat transfer on a small vertical heated surface in an impinging circular liquid jet, Heat Transfer Science and Technology, Hemisphere Publishing Corp., 1988, pp. 193–200.

[20] V.V. Calmidi, R.L. Mahajan, The effective thermal conductivity of high porosity fibrous metal foams, ASME J. Heat Transfer 121 (1999) 466–471.

[21] S.L. Lee, A strong implicit solver for two-dimensional elliptic differential equations, Numer. Heat Transfer Part B 16 (1989) 161–178.

[22] B.V. Antohe, J.L. Lage, A general two-equation macroscopic turbulence model for incompressible flow in porous media, Int. J. Heat Mass Transfer 40 (1997) 3013–3024.

[23] M. Prakash, Özden F. Turan, Y. Li, J. Mahoney, G.R. Thorpe, Impinging round jet studies in a cylindrical enclosure with and without a porous layer: Part I—flow visualisations and simulations, Chem. Eng. Sci. 56 (2001) 3855–3878.

[24] R. Gardon, J. Akfirat, Heat transfer characteristics of impinging two-dimensional air jets, ASME J. Heat Transfer 88 (1966) 101–108.

[25] D.C. Wadsworth, I. Mudawar, Cooling of a multichip electronic module by mean of confined two-dimensional jets of dielectric liquid, ASME J. Heat Transfer 112 (1990) 891–898.